Bulletin of Applied Mathematics and Mathematics Education
Vol. 6, No. 1, April 2026, pp. 1–10
e-ISSN: 2776-1029 p-ISSN: 2776-1002 DOI: 10.12928/bamme.v6i1.14695

APPLIED MATHEMATICS

Data assimilation for predicting the dynamics of acute respiratory infections using the ensemble Kalman filter

Yolanda Norasia [1,*], Dinni Rahma Oktaviani [1], Aini Fitriyah [2], Devi Marita Putri [1]

[1] Universitas Islam Negeri Walisongo, Jl. Prof. Hamka, Ngaliyan, Semarang 50185, Indonesia
[2] University of Birmingham, Birmingham B15 2TT, United Kingdom
*Corresponding author

Abstract

Acute respiratory infection (ARI) is one of the most pressing public health problems due to its high transmission rate and the potential to cause significant pressure on health services. This study applies the Ensemble Kalman Filter (EnKF) method to predict the spread of ARI with a three-compartment population model, namely Susceptible (S), Exposed (E), and Infected (I). This study shows that the EnKF method can predict the spread of ARI well. The number of ensembles used affects the level of accuracy. The EnKF provides accurate predictions of the dynamics of ARI spread, making it relevant as a scientific basis in the formulation of data-based mitigation strategies. It can provide a scientific basis for policymakers to formulate accurate and measurable preventive measures.

Keywords: ARI, data assimilation, ensemble Kalman filter

How to cite: Norasia, Y., Oktaviani, D. R., Fitriyah, A., & Putri, D. M. (2026). Data assimilation for predicting the dynamics of acute respiratory infections using the ensemble Kalman filter. *Bulletin of Applied Mathematics and Mathematics Education, 6*(1), 1–10. https://doi.org/10.12928/bamme.v6i1.14695

Article history: Received 10/10/2025, Accepted 20/04/2026, Published 02/06/2026

Correspondence address: Universitas Islam Negeri Walisongo, Jl. Prof. Hamka, Ngaliyan, Semarang 50185, Indonesia.
E-mail: yolandanorasia@walisongo.ac.id

INTRODUCTION

Acute respiratory infection (ARI) is a disease that attacks the upper or lower respiratory tract caused by viruses and bacteria. Viruses that cause ARI include influenza, enterovirus, respiratory syncytial virus, and adenovirus (Inderiati et al., 2023). Bacteria that often cause ARI include *Streptococcus pneumoniae*, *Haemophilus influenzae*, and *Mycoplasma pneumoniae* (Goraahe et al., 2025). Hot weather and the density of Hajj pilgrims are known to trigger a spike in ARI cases, especially since several dangerous ARI categories, such as SARS-CoV and new influenza, have the potential to have a major impact on global health. This is in line with the WHO Interim Guidelines, which state that ARI can be transmitted from human to human with symptoms varying from mild to fatal, depending on the type of pathogen, environmental factors, and host conditions. The risk of ARI transmission increases when Hajj pilgrims gather in large numbers, and strict preventive measures must be taken. The Indonesian Ministry of Health stated that drastic changes in temperature and humidity make viruses and bacteria thrive (Rahmadanti & Alnur, 2023). Based on 2019 WHO data, ARI contributes to reducing the life expectancy of sufferers. This situation further reinforces the importance of preventing the ARI spread. One way of doing this is by predicting its spread. Predictions can serve as a basis for future policy planning.

The application of data assimilation in predicting the ARI spread is a relevant approach. Through the process of integrating data with epidemiological models, the Kalman Filter can produce continuous prediction results, resulting in a more accurate picture of the ARI spread. The application of the Kalman Filter in epidemiological models has been applied to the COVID-

19 spread in Bangladesh (Islam et al., 2020). The study showed that the short-term COVID-19 prediction results for four months were stable. Predictions of mortality among COVID-19 patients have been conducted using the Kalman Filter. The study showed that the Kalman Filter can be applied to uncontrolled sample sizes and class distributions (Liu et al., 2024). Not only in the field of epidemiology, the Kalman Filter can also be applied in underwater navigation systems used for military and civilian purposes (Xincun et al., 2013). One of the advantages of the Kalman Filter is its ability to produce estimates of system conditions without requiring large amounts of historical data. The Kalman Filter works recursively, namely by utilizing information from current conditions, system models, and the latest observation data to update predictions.

The epidemiological spread diseases are difficult to model accurately due to the uncertainty and nonlinear nature of real phenomena. The Kalman Filter is designed for linear systems with a Gaussian error distribution, making it less suitable for application to epidemiological models. The Kalman filter was developed to adapt to the characteristics of the system being observed. To address nonlinear problems, methods used include the Extended Kalman Filter and the Ensemble Kalman Filter.

Extended Kalman Filter (EKF) method is a modified Kalman Filter that linearizes nonlinear models using a Taylor series approach and a Jacobian matrix (Diniz, 2020). The epidemiological model with the addition of reinfection rates and social distancing factors was predicted using the EKF (Zhu et al., 2021). The model used in this study is the SEIRD model, which contains five compartments consisting of Susceptible, Exposed, Infection, Recovered, and Decreased. EKF performance decreases when a nonlinear system is being modeled (Diniz, 2020). To overcome this problem, Gair Evensen developed the Ensemble Kalman Filter (EnKF) method using a Monte Carlo approach by generating several ensembles to estimate the mean and covariance, resulting in more accuracy and efficiency in large-dimensional nonlinear systems (Evensen, 1994).

A study comparing EKF and EnKF conducted on the Sobek River hydrodynamic model showed that EnKF with 10 ensembles required approximately 0.8 times the computational time of EKF (El Serafy & Mynett, 2004). Research on BLDC/Brushless DC Motor speed prediction showed that EnKF was able to provide more accurate predictions than EKF (Rifan et al., 2015). Jang et al.'s study utilized EnKF in a mathematical model of the HBV/Hepatitis B spread infection to formulate an optimal treatment strategy that balances therapeutic effectiveness and cost (Jang et al., 2018). The results of the study's numerical simulations showed that drugs that inhibit HBV virus production are more effective in reducing viral load than drugs that inhibit new infections. The application of EnKF to the COVID-19 spread was used to estimate changes in interaction parameters between susceptible and infected populations (Engbert et al., 2021). The results show that after social interventions such as school closures and interaction restrictions, contact parameter values decreased significantly between March 17-19 and March 31-April 2. In other words, social distancing policies have been effective in suppressing the COVID-19 spread.

ARI is a disease with a high incidence that can have serious impacts, especially on children and vulnerable individuals. The rapid ARI spread requires data-driven prevention and control strategies, so that implemented policies are truly effective in suppressing the rate of disease spread. Previous studies have shown that EnKF is an appropriate method for predicting the dynamics of infectious disease spread. The EnKF method was used in this study because it has good capabilities in solving nonlinear problems in large-dimensional systems. Furthermore, there has been no research that applies the EnKF method to the SEI model for ARI problems. Therefore, this study focuses on the application of EnKF with ensemble variations on the rate of change of each SEI population using MATLAB software, thereby providing a scientific basis for formulating more targeted ARI prevention and control strategies.

RESEARCH METHOD

Mathematical model of the ARI spread

The ARI spread model consists of three populations: SEI, S, which is the population susceptible to ARI, E, which is the population exposed to ARI, and I, which is the population infected with ARI. The mathematical model of ARI spread is given as follows (Kumari & Sharma, 2018).

$$\frac{dS}{dt} = mA - \theta S - \lambda SI + n\xi I - \mu S \quad (1)$$

$$\frac{dE}{dt} = m'A - \theta S - \lambda(1 + \delta\lambda')EI + n'\xi I - \mu E \quad (2)$$

$$\frac{dI}{dt} = \lambda SI + \lambda(1 + \delta\lambda')EI - (\xi + \phi + \mu)I \quad (3)$$

with $m' = 1 - m$, $\lambda' = 1 - \lambda$ and $n' = 1 - n$.

The ARI transmission model is a continuous-time dynamic system that describes changes in the number of infected individuals over time. The initial value of each population is $S_0 = 2864$, $E_0 = 68.87$, and $I_0 = 9528$ (Kumari & Sharma, 2018). This value is used as the initial value in building a dynamic system model before the estimation process is carried out. In the EnKF application, the ARI transmission model is transformed into a discrete-time dynamic system using discretization, allowing prediction calculations and updates to be performed iteratively at specific time intervals (Pedroso et al., 2022). The discretization method used is forward finite difference, namely the time derivative is approximated by $\frac{dS}{dt} = \frac{S_{k+1} - S_k}{\Delta t}$ and the recursive form $S_{k+1} = S_k + \Delta t\, f(S_k)$.

Implementation of Ensemble Kalman Filter method (EnKF)

The implementation of the EnKF method consists of four steps, namely determining the system model and measurement, initiation, prediction, and correction, as follows.

Determining the system model and measurements

System model:

$$x_{k+1} = f(x_k, u_k) + w_k \quad (4)$$

with system noise $w_k \sim N(0, Q_k)$.

Measurement model:

$$z_k = Hx_k + v_k \quad (5)$$

with system noise $v_k \sim N(0, R_k)$

The process noise covariance matrix and observation noise covariance, namely Q=0.0001 and R=0.0001, assume that the uncertainty in the model is relatively small so that the model can represent real phenomena (Katzfuss et al., 2016; Keller et al., 2018).

Initiation

The initialization step using the EnKF method involves providing initial input to generate N ensembles (Moldovan, 2021).

$$x_{0,i} = x_0 + w_i \quad (6)$$

Determining the mean of the N ensembles (Sánchez-León et al.,2020; van Leeuwen, 2020).

$$\hat{x}_{0,i} = \frac{1}{N}\sum_{i=1}^{N} x_{0,i}$$

Prediction
Each ensemble state is updated to the next time using the dynamic system model for ARI spread, for the -*i* th ensemble with (Roth et al., 2017; Jin et al., 2026).

$$\hat{x}_k^- = f\left(\hat{x}_{k-1,i}^-, u_{k-1,i}\right) + w_{k,i} \tag{7}$$

After all ensembles are calculated, the mean prediction $\hat{x}_{k,i}^- = \frac{1}{N}\sum_{i=1}^{N} \hat{x}_{k,i}^-$ and the covariance of the prediction error $P_{k+1}^- = \frac{1}{N-1}\sum_{i=1}^{N}\left(\hat{x}_{k,i}^- - \hat{x}_k^-\right)\left(\hat{x}_{k,i}^- - \hat{x}_k^-\right)^T$.

Correction
Correction steps are taken after the prediction is complete to ensure more accurate prediction results. The first step is to generate a set of N measurement data (De Korte et al., 2025).

$$z_{k,i} = z_k + v_{k,i} \tag{8}$$

Next, calculate the Kalman Gain to determine the weighting between the predicted results and the observed data $K_k = P_k^- H^T (H P_k^- H^T + R_k)^{-1}$. Each ensemble member is updated using the Kalman Gain $\hat{x}_{k,i} = \hat{x}_{k,i}^- + K_k(z_{k,i} - H\hat{x}_{k,i}^-)$. From the correction results for each ensemble member, the mean prediction $\hat{x}_{k,i} = \frac{1}{N}\sum_{i=1}^{N} \hat{x}_{k,i}$ and the covariance of the prediction error $P_k = [I - K_k H]P_k^-$.

Ensemble Kalman Filter method (EnKF) analyzing simulation results of ARI spread
The ARI spread based on the population change rates S, E, and I over time was simulated using the EnKF method. The ensemble variations for predicting the ARI spread are 50, 100, 200, and 300 ensembles. The accuracy of the ARI spread prediction using the EnKF method was evaluated using the Root Mean Square Error (RMSE). This measure is obtained by comparing the observed data for each compartment S, E, and I with the mean value of the ensemble predictions (Nasution et al., 2022). A lower RMSE indicates higher accuracy of the model's predictions (Zulfi et al., 2018).

RESULTS AND DISCUSSION

To apply the EnKF method to the ARI spread, a mathematical model formulation in the form of a discrete dynamic system is first required. This model is derived from the SEI model, considering individual interaction factors, environmental impacts, and other relevant epidemiological parameters. Discretization is performed to adapt the continuous system to the discrete-time EnKF framework. Once the SEI model is discretized, the next step is to define the measurement model and initialize the ensemble, which forms the basis for the prediction and correction stages of the EnKF method. The discretization of the ARI spread model in the SEI model is as follows.

$$S_{k+1} = mA\,\Delta t - \theta S_k\,\Delta t - \lambda S_k I_k\,\Delta t + n\xi I_k - \mu S_k\,\Delta t + S_k \tag{9}$$

$$E_{k+1} = (1-m)A\Delta t - \theta S_k \Delta t - \lambda(1+\delta\lambda')E_k I_k \Delta t + (1-n)\xi I_k - \mu E_k \Delta t - E_k \tag{10}$$

$$I_{k+1} = \lambda S_k I_k \Delta t + \lambda(1+\delta\lambda')E_k I_k \Delta t - (\xi + \phi + \mu) I_k \Delta t + I_k \tag{11}$$

So, the ARI spread system model is

$$\begin{pmatrix} S \\ E \\ I \end{pmatrix}_{k+1} = \begin{pmatrix} 1 + \left(-\theta - \lambda x_{2_{(k)}} - \mu\right)\Delta t & \left(-\lambda x_{1_{(k)}}\right)\Delta t & (n\xi)\Delta t \\ \theta\Delta t & \left(-\lambda(1+\delta\lambda')x_{3_{(k)}} - \mu\right)\Delta t + 1 & \left(-\lambda(1+\delta\lambda')x_{2_{(k)}} + (1-n)\xi\right)\Delta t \\ \lambda x_{3_{(k)}} & \left(\lambda(1+\delta\lambda')x_{3_{(k)}}\right)\Delta t & \left(-\lambda(1+\delta\lambda')x_{2_{(k)}} - (\xi+\phi+\mu)\Delta t + 1\right) \end{pmatrix} + w_k \tag{12}$$

with $w_k \sim N(0, Q_k)$. The measurement model for ARI spread is

$$z_k = (0 \quad 1 \quad 0)\begin{pmatrix} S_k \\ E_k \\ I_k \end{pmatrix} + v_k \tag{13}$$

with $v_k \sim N(0, Q_k)$. The next step is the initialization of EnKF which is to generate several N ensembles for each state as follows.

$$x_{k,i} = \begin{pmatrix} S_0 \\ E_0 \\ I_0 \end{pmatrix} + w_k \tag{14}$$

with the mean of each state of the ensemble generator $\hat{x}_0 = \begin{pmatrix} \hat{S}_0 \\ \hat{E}_0 \\ \hat{I}_0 \end{pmatrix}$.

Next is the prediction step as follows.

$$\hat{x}_{k,i}^- = \begin{pmatrix} \hat{S}_{k-1} \\ \hat{E}_{k-1} \\ \hat{I}_{k-1} \end{pmatrix} + \begin{pmatrix} w_{1,i} \\ w_{2,i} \\ w_{3,i} \end{pmatrix} \tag{15}$$

The mean prediction $\hat{x}_{k,i}^- = \frac{1}{N}\sum_{i=1}^{N} \hat{x}_{k,i}^-$ and the covariance error $P_{k+1}^- = \frac{1}{N-1}\sum_{i=1}^{N}\left(\hat{x}_{k,i}^- - \hat{x}_k^-\right)\left(\hat{x}_{k,i}^- - \hat{x}_k^-\right)^T$ and correction step as follows.

$$\hat{x}_{k,i} = \hat{x}_{k,i}^- + K_k\left(z_{k,i} - H\hat{x}_{k,i}^-\right) \tag{16}$$

with the mean prediction $\hat{x}_{k,i} = \frac{1}{N}\sum_{i=1}^{N} \hat{x}_{k,i}$ and the covariance error $P_k = [I - K_k H]P_k^-$.

The EnKF method is applied to the ARI spread model for populations S, E, and I. In predicting the spread of ARI, several parameters are used, such as the birth rate A, the birth probability m, the interaction of susceptible with infected λ, the scale environmental δ, the impact of pollution λ', the movement rate of susceptible individuals θ, the natural death rate μ, the interaction rate of exposed individual with infected ξ, the death rate of infected individual ϕ, and the rate healthy individuals becoming susceptible n. In predicting the ARI spread, initial values are $S_0 = 2864; E_0 = 68.87; I_0 = 9528$ (Kumari & Sharma, 2018), (data.jatengprov.go.id). Error in the ARI prediction results are calculated using Root Mean Square Error (RMSE).

Figure 1 shows the rate of change of the susceptible population S to the ARI spread using EnKF with variations in the number of ensembles N=50, 100, 200, and 300. The rate of the S population experienced an initial increase from days 0 to 25. This phenomenon occurs because at the beginning of the ARI spread stage, some of the population is still in a susceptible condition before moving to the infected category I or exposed E. The S population experienced a gradual decrease as the number of exposed or infected individuals increased from days 120 to 180. Across variation in N, the prediction results were consistent with the observed data patterns. However, if observed in detail, the estimate with N = 50 appears to be closest to the observed data patterns. This is also shown through the RMSE calculation in Table 1, the RMSE value of the S population for N = 50 is RMSE 0.0651 smaller than N = 100 (0.076), N = 200 (0.0687), and N = 300 (0.0672). These results indicate a trade-off between computational complexity and prediction accuracy. Although increasing the number of ensembles (N=100, 200, 300) can improve the stability of the EnKF process, the accuracy improvement obtained is not significant compared to N=50. In other words, a relatively small ensemble size is sufficient to obtain reliable predictions while maintaining computational efficiency.

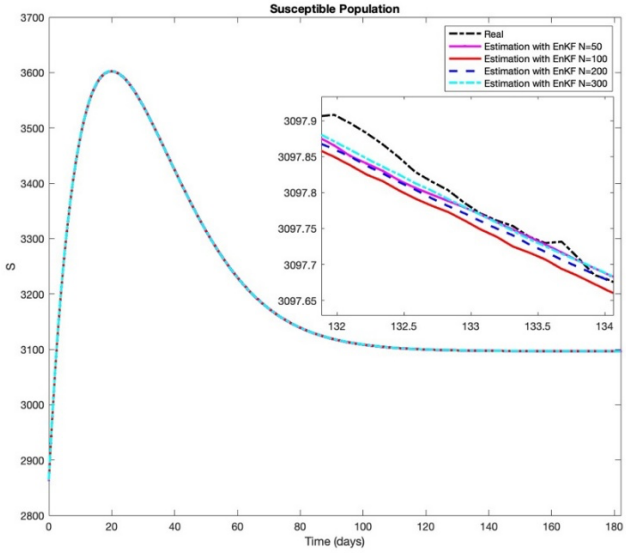

Figure 1. Prediction of susceptible population dynamics in ARI spread with varying ensemble sizes ($N = 50, 100, 200, and\ 300$).

Figure 2 shows that the exposed population E increased at the initial time, then decreased until it reached stability by day 180. The increase in the exposed population was caused by the transition process of the S population infected with the ARI virus but not yet showing symptoms. In other words, susceptible individuals exposed to the virus will move into the exposed population so that the number of exposed individuals increases sharply in the initial period. The E population decreased as the infected population I entered. Based on these predictions, ensemble variations produce results that are not conducive to approaching the observed data. It is also supported by the RMSE value in Table 1, resulting in a very small error of 0.0082-0.0134. The smallest RMSE value was obtained at N = 100, 200, and 300 with the same value of 0.0082. Increasing the number of ensembles resulted in more stable and convergent predictions.

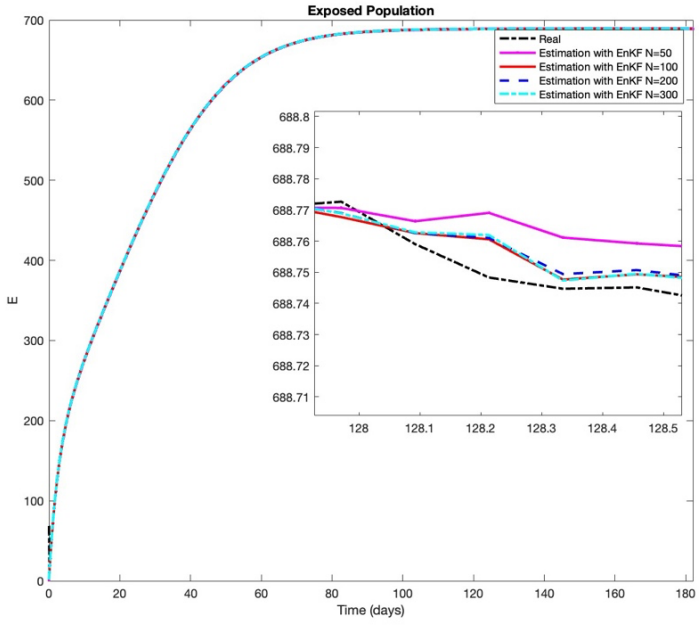

Figure 2. Prediction of exposed population dynamics in ARI spread with varying ensemble sizes (N=50, 100, 200, and 300)

Figure 3 shows the pattern of decline in the population infected with I after reaching its peak. In the initial phase of the spread of ARI, individual S had moved to population E and then to I. However, over time, the number of susceptible individuals decreased so that the rate of new transmission decreased. The EnKF method was able to track the rate of change in the population infected with I quite well. The RMSE value in Table 1 shows that N = 300 gives the smallest error of 0.0807. Therefore, N = 300 provides the most accurate results in representing the rate of population decline I compared to smaller N sizes.

The parameters λ, δ, and θ have different effects on the dynamics of the spread of ARI. The parameter λ has the most significant effect because it appears in the interaction of $\lambda SI + n\xi I - \mu S$ and $\lambda(1 + \delta\lambda')EI$. In other words, a small increase in the parameter λ can increase the population infected. The parameter δ acts as a reinforcing factor for the spread through $1 + \delta\lambda'$. Then, the parameter acts as a controlling factor because it can have a negative effect by reducing the population at S and E.

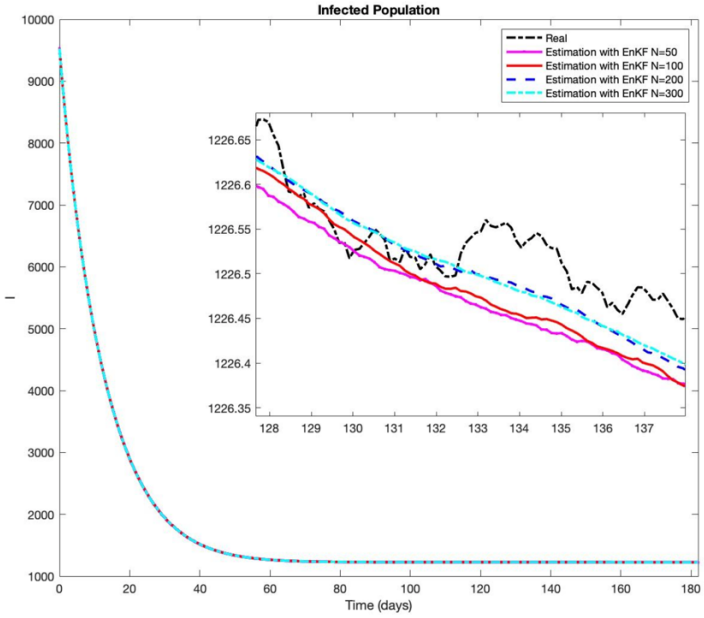

Figure 3. Prediction of infected population dynamics in ARI spread with varying ensemble sizes ($N = 50, 100, 200, and\ 300$).

This information is important for the government in formulating policies to control the ARI spread. Prevention strategies for the spread of the virus can include implementing policies such as social restrictions, which are represented in the ARI model by reducing λ and δ. Furthermore, policy reinforcement can be represented by mobility monitoring by increasing the θ parameter. These changes can contribute to lowering the peak of infections, accelerating outbreak control, and reducing the spread of ARI. This helps support data-driven decision-making. Planned policies can be directed at early prevention, more efficient allocation of health resources, and adaptive mitigation strategies.

Table 1. RMSE of EnKF predictions for SEI populations

Population	RMSE EnKF N-50	RMSE EnKF N-100	RMSE EnKF N-200	RMSE EnKF N-300
S	0.0651	0.0726	0.0687	0.0672
E	0.0134	0.0082	0.0082	0.0082
I	0.0862	0.0809	0.0820	0.0807

CONCLUSION

Based on the simulation results and analysis of the prediction of the ARI spread using the EnKF method in populations S, E, d, and I, it was found that the EnKF method was able to represent the spread of the disease well in various variations in the number of ensembles. Population S showed that a small number of ensembles, N = 50, was sufficient to provide accurate predictions with the smallest RMSE value of 0.0651. In population E with N = 100, 200, and 300, it produced more stable predictions and the smallest error of 0.0082. In population I, the best prediction results were achieved at N = 300 with an RMSE of 0.0807. The results show a trade-off between accuracy and computational complexity, where the choice of ensemble size needs to be adjusted to the objectives of the analysis. From a policy perspective, the EnKF prediction results in this study can be a basis for the government to design mitigation strategies for the spread of ARI, such as strengthening programs to prevent the spread of ARI in the early phase, increasing early detection in population E, and optimizing health resources to handle population I.

The limitation of this study lies in the use of a simple model, which only utilizes three compartments: Susceptible, Exposed, and Infection. This model does not fully describe the healing process, the likelihood of re-infection, and the demographic factors that influence transmission. Therefore, the study of the spread of ARI is interesting and warrants further development. The ARI transmission model can be developed by adding other compartments to better represent epidemiological phenomena closer to real-world ones.

ACKNOWLEDGEMENT

Not available.

DECLARATION

Author contribution

All authors contribute in the research and/or writing the paper, and approved the final manuscript.

Yolanda Norasia	Conceptualizing the research idea, leading the investigation, and setting up the methodology.
Dinni Rahma Oktaviani	Assisting the investigation, reviewing the validity of the methodology, analyzing the data, and writing the original draft.
Aini Fitriyah	Assisting the investigation, reviewing the paper, enriching the data analysis, and translating the paper into English.
Devi Marita Putri	Assisting the investigation, collecting and organizing the research data, and proofreading the manuscript.

Funding

This research did not receive any funding.

Conflict of interest

All authors declare that they have no competing interests.

Ethics declaration

We as authors acknowledge that this work has been written based on ethical research that conforms with the regulations of our institutions and that we have obtained the permission from the relevant institutes when collecting data. We support the Bulletin of Applied Mathematics and Mathematics Education (BAMME) in maintaining the high standards of personal conduct, practicing honesty in all our professional practices and endeavors.

The use of artificial intelligence

We do not use any generative AI tools to write any part of this paper.

Additional information

Not available.

REFERENCES

de Korte, C. W. E., Verlaan, M., & Heemink, A. W. (2025). A wave data assimilation system for the North Sea based on Ensemble Kalman Filtering and the potential of satellite altimetry. *Ocean Modelling*, *197*, 102586. https://doi.org/10.1016/j.ocemod.2025.102586

Diniz, P. S. R. (2020). *Adaptive Filtering Algorithms and Practical Implementation Fifth Edition*. https://doi.org/10.1007/978-3-030-29057-3

El Serafy, G. Y., & Mynett, A. E. (2004). Comparison of EKF and EnKF in Sobek river: Case study maxau-ijssel. *Hydroinformatics*, 513–520.

Engbert, R., Rabe, M. M., Kliegl, R., & Reich, S. (2021). Sequential data assimilation of the stochastic SEIR epidemic model for regional COVID-19 dynamics. *Bulletin of Mathematical Biology*, *83*(1). https://doi.org/10.1007/s11538-020-00834-8

Evensen, G. (1994). Sequential data assimilation with a nonlinear quasi-geostrophic model using Monte Carlo methods to forecast error statistics. *Journal of Geophysical Research*, *99*(C5). https://doi.org/10.1029/94jc00572

Nasution, A. F., Lubis, R. S., & Widyasari, R. (2023). Implementation of the Generalized Space Time Autoregressive (GSTAR) model in the case of the spread of coronavirus in the district city of North Sumatra. *ZERO: Jurnal Sains, Matematika dan Terapan*, *6*(2), 157-166.

Goraahe, N., Haruna, N., Sakinah4, A. I., & Ahmad, A. (2025). Profil bakteri dari usap tenggorok penderita infeksi saluran pernapasan usia sekolah dasar di Puskesmas Tamalanrea Makassar. *Jurnal Riset Rumpun Ilmu Kedokteran*, *4*(1), 1–9. https://doi.org/10.55606/jurrike.v4i1.4313

Inderiati, D., Rachmawaty, T., & Amaniah Anhar, C. (2023). Identification of acute respiratory infection patients using RP2 nested multiplex PCR test in Jakarta, Indonesia. *Medical Laboratory Technology Journal, 8*(2), 53-62. https://doi.org/10.31964/mltj.v8i2.519

Islam, M. S., Hoque, M. E., & Amin, M. R. (2020). Integration of Kalman filter in the epidemiological model: a robust approach to predict COVID-19 outbreak in Bangladesh. *International Journal of Modern Physics C, 32*(8), 2150108. https://doi.org/10.1142/S0129183121501084

Jang, J., Jang, K., Kwon, H. D., & Lee, J. (2018). Feedback control of an HBV model based on ensemble kalman filter and differential evolution. *Mathematical Biosciences and Engineering*, *15*(3), 667–691. https://doi.org/10.3934/mbe.2018030

Jin, Y., Chen, G., & Tian, Z. (2026). Investigation of ensemble Kalman filter-based data assimilation for turbulent flow in a 3×3 rod bundle. *Nuclear Engineering and Technology*, *58*(2), 103899. https://doi.org/10.1016/j.net.2025.103899

Katzfuss, M., Stroud, J. R., & Wikle, C. K. (2016). Understanding the ensemble Kalman filter. *The American Statistician, 70*(4), 350-357. https://doi.org/10.1080/00031305.2016.1141709

Keller, J., Hendricks Franssen, H. J., & Marquart, G. (2018). Comparing seven variants of the ensemble Kalman filter: How many synthetic experiments are needed? *Water Resources Research*, *54*(9), 6299–6318. https://doi.org/10.1029/2018WR023374

Kumari, N., & Sharma, S. (2018). Modeling the dynamics of infectious disease under the influence of environmental pollution. *International Journal of Applied and Computational Mathematics*, *4*(3). https://doi.org/10.1007/s40819-018-0514-x

Liu, J., Kirkland, L., & Srivastava, J. (2024). A Kalman filter based framework for monitoring the performance of in-hospital mortality prediction models over time. http://arxiv.org/abs/2402.06812

Moldovan, G., Lehnasch, G., Cordier, L., & Meldi, M. (2021). A multigrid/ensemble Kalman filter strategy for assimilation of unsteady flows. *Journal of Computational Physics, 443*, 110481.

Pedroso, L., Batista, P., Oliveira, P., & Silvestre, C. (2022). Discrete-time distributed Kalman filter design for networks of interconnected systems with linear time-varying dynamics. *International Journal of Systems Science, 53*(6), 1334–1351. https://doi.org/10.1080/00207721.2021.2002461

Rahmadanti, D., & Alnur, R. D. (2023). Faktor-faktor yang berhubungan dengan kejadian ISPA pada balita. *Jurnal Sains dan Kesehatan*, *2*(2), 63-70. https://doi.org/10.57151/jsika.v2i2.266

Rif'an, M., Yusivar, F., Wahab, W., & Kusumoputro, B. (2015). A comparison of ensemble Kalman filter and extended Kalman filter as the estimation system in sensorless BLDC motor. *ARPN Journal of Engineering and Applied Sciences*, *10*(17), 7386-7393.

Roth, M., Hendeby, G., Fritsche, C., & Gustafsson, F. (2017). The ensemble Kalman filter: A signal processing perspective. *Eurasip Journal on Advances in Signal Processing, 2017*(1). https://doi.org/10.1186/s13634-017-0492-x

Sánchez-León, E., Erdal, D., Leven, C., & Cirpka, O. A. (2020). Comparison of two ensemble Kalman-based methods for estimating aquifer parameters from virtual 2-D hydraulic and tracer tomographic tests. *Geosciences (Switzerland)*, *10*(7), 1–27. https://doi.org/10.3390/geosciences10070276

van Leeuwen, P. J. (2020). A consistent interpretation of the stochastic version of the ensemble Kalman filter. *Quarterly Journal of the Royal Meteorological Society*, *146*(731), 2815–2825. https://doi.org/10.1002/qj.3819

Xincun, Y., Yongzhong, O., Fuping, S., & Hui, F. (2013). Kalman filter applied in underwater integrated navigation system. *Geodesy and Geodynamics*, *4*(1), 46-50.

Zhu, X., Gao, B., Zhong, Y., Gu, C., & Choi, K. S. (2021). Extended Kalman filter based on stochastic epidemiological model for COVID-19 modelling. *Computers in Biology and Medicine*, *137*. https://doi.org/10.1016/j.compbiomed.2021.104810

Zulfi, M., Hasan, M., & Purnomo, K. D. (2018). The development rainfall forecasting using kalman filter. *Journal of Physics: Conference Series*, *1008*(1). https://doi.org/10.1088/1742-6596/1008/1/012006